Geomechanics and Engineering, *Vol. 39, No. 1 (2024) 73-85*
https://doi.org/10.12989/gae.2024.39.1.073

Evaluation of artificial ground freezing behavior considering the effect of pore water salinity

Gyu-Hyun Go[1], Dinh-Viet Le[1] and Jangguen Lee*[2]

[1]*Department of Civil Engineering, Kumoh National Institute of Technology, 61, Daehak-ro, Gumi-si, Gyeongsangbuk-do, Republic of Korea*
[2]*Department of Future & Smart Construction Research, KICT, 283, Goyang daero, Ilsanseo gu, Goyang si, Gyeonggi do, Republic of Korea*

(*Received January 22, 2024, Revised August 16, 2024, Accepted September 13, 2024*)

Abstract. There is growing interest in introducing artificial ground freezing (AGF) as a method to temporarily secure unstable ground during tunnel construction. In order to efficiently operate an artificial ground freezing system, basic modeling research is needed on the changes in freezing behavior according to various soil environmental conditions as well as design conditions. In this study, a thermal-hydraulic coupled analysis was performed to simulate the artificial ground freezing process of ground containing salt water. The effect of major variables, including pore water salinity, on artificial ground freezing test performance was investigated. Additionally, an artificial neural network-based prediction model was proposed to estimate the time required to achieve the desired arch thickness. The artificial neural network model demonstrated reliable accuracy (R^2 = 0.9942) in predicting the time it would take to reach the desired arch thickness. Among the major input variables considered, pore water salinity appeared to be the most influential input variable, and initial soil temperature showed the least importance.

Keywords: artificial ground freezing; artificial neural network; numerical simulation; pore water salinity

1. Introduction

Recently, with rapid industrial development and the acceleration of underground space development in cities, the demand for underground tunnel construction in densely populated areas is increasing. Tunnel construction in areas with dense residential zones and diverse underground infrastructure is particularly challenging. In addition, the number of cases where tunnel construction becomes inevitable, even in difficult sites with poor ground conditions, is on the rise. Therefore, it has become crucial to smoothly execute tunneling construction by selecting effective and appropriate auxiliary methods (Reza and Erdal 2009, Wang *et al*. 2019a, Tacim *et al*. 2023, Li *et al*. 2016, Naithani *et al*. 2022, Zhou *et al*. 2023, Osgoui and Ünal 2009). While various auxiliary methods are available for reinforcing soft ground in challenging construction sections, the artificial ground freezing technique is commonly employed as a powerful and effective construction method, which offers support to the ground, controls groundwater, and stabilizes structures throughout the construction process (Cicchetti 2018). The artificial ground freezing (AGF) technique involves circulating refrigerants in freeze pipes buried in a soft ground, which freezes the ground and creates ice pillars, and frozen wall around the pipes (Fig. 1).

In comparison with other geotechnical support methods, AGF is not limited to a specific ground type (Alzoubi *et al.* 2020) and can be applicable to fine-grained soil such as silt and clayey sand (Zhou and Tang 2018) or fractured sedimentary rocks such as sandstone (Shen *et al*. 2018).

Compared to non-frozen soil, frozen soil has higher strength and lower permeability coefficient, making stable ground excavation construction possible (Sres 2009). The artificial freezing method is known to be a more effective method when applied to ground with a weak tunnel face or severe groundwater leakage because it has superior water blockage compared to existing methods such as grouting or diaphragm wall (Pimentel *et al*. 2012). As the artificial ground freezing method can enhance the ground stability without negative environmental impacts, its usage is predicted to gradually increase (Cicchetti 2018, Andersland and Ladanyi 2004, Schmall and Dawson 2017). Recently, there has been an increasing focus on using cost-effective and reliable state-of-the-art construction techniques to ensure the safety and effectiveness of excavation projects in urban centers. Considering these circumstances, establishing a reliable performance evaluation technology for artificial ground freezing is essential for universal application of this technology.

Several field demonstration tests have been carried out. For example, Crippa and Manassero (2006) presented results of ground temperature changes based on the type of refrigerant used for an artificial ground freezing system applied in Sophiaspoor Tunnel in Netherlands. Additionally, Papakonstantinou *et al*. (2013) analyzed the key factors affecting the ground-freezing behavior using an artificial ground-freezing system constructed in the Naples subway in Italy. Han *et al*. (2016) analyzed the effect of the frost heave pressure generated by artificial ground freezing

*Corresponding author, Ph.D.
E-mail: jlee@kict.re.kr

ISSN: 2005-307X (Print), 2092-6219 (Online)

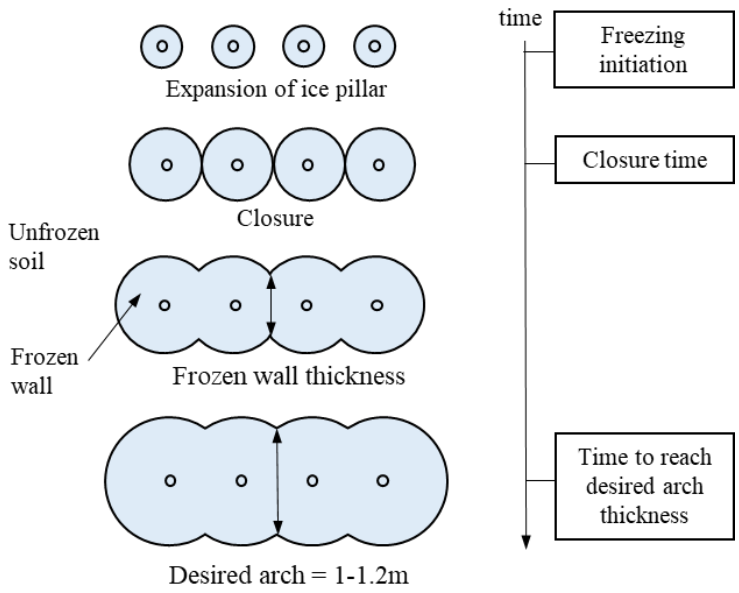

Fig. 1 Schematic of the artificial ground freezing stages

through a demonstration test in Yangtze River Tunnel in Shanghai, China.

Numerical analyses have also been carried out in addition to field verification tests. Hansson *et al*. (2004) proposed a numerical analysis model that considered the phase change of pore water generated during the ground freezing process. The calculated analysis results were compared and verified using experimental data. Later, Tan *et al*. (2011) established a Thermal-Hydraulic coupled analysis technique based on continuum mechanics, thermodynamics, and segregation potential theory, while McKenzie *et al*. (2007) and Kurylyk *et al*. (2014) presented a numerical analysis model that considered the effect of groundwater flow, and then verified the model using the analytical solution proposed by Lunardini (1998). Jin *et al*. (2021) conducted experimental and numerical investigations of closure time during artificial ground freezing under vertical flow condition. In addition to theses, numerous numerical analysis studies have been carried out on the effects of pore water phase change, changes in mechanical properties due to freezing, and groundwater flow (Pimentel *et al*. 2012, Vitel *et al*. 2016, Marwan *et al*. 2016, Huang *et al*. 2018, Shin *et al*. 2018, Li *et al*. 2019).

Although previous studies related to artificial ground freezing have yielded great research achievements, most of those studies have not focused on seabed ground conditions like salinity of pore-water. As the number of subsea tunnel construction projects worldwide increases, there is an increasing demand to understand ground freezing techniques used in subsea tunnels. The research associated with modeling that considers the geo-environmental conditions of the seabed can aid in the precise design of artificial ground freezing system, ultimately improving the reliability and cost-effectiveness of such construction and operation. Although some studies have analyzed the thermal-hydraulic-mechanical behavior of soil based on a porewater salinity at the specimen scale (Tounsi *et al*. 2020, Wu *et al*. 2015) few studies have investigated the impact of the pore water salinity on artificial ground freezing applications. As the salinity of pore water can affect the ground freezing behavior, including changes in the thermal characteristics of soil, numerical simulation studies that consider these factors can be of significance.

To address the insufficient research on the impact of the pore water salinity on the artificial ground freezing behavior, in this study, we modeled the artificial ground freezing process in a saturated soil bed containing saltwater. After validation of the model with testing data, we evaluated the performance of the artificial ground freezing in the field scale soil domain. Then, a parametric study was carried out to analyze the variables that affect the formation of design ice walls. Lastly, based on the dataset from the parametric study, a artificial neural network based prediction model was proposed to estimate the time needed for achieving a desired arch thickness more practically.

2. Methodology

2.1 Finite element analysis

To simulate the artificial ground freezing process, a finite-element model was constructed based on the thermodynamic theory (Coussy 2010, Coussy and Monteiro 2017). The constitutive relations of which were derived and implemented in the weak form PDE module of Comsol Multiphysics, a commercial FE program (Comsol 2024). In this study, the ground was assumed to be a saturated sandy soil stratum with a three-phase structure comprising of soil particles, water, and ice. Assuming a local temperature equilibrium state, the ground temperature change caused by freezing can be simulated using the following energy conservation equation (Coussy and Poromechanics 2004, Michalowski and Zhu 2006)

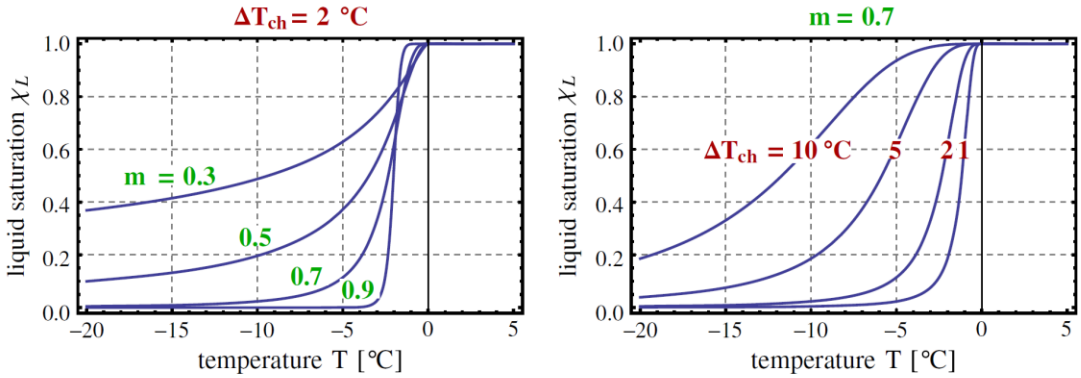

Fig. 2 Unfrozen liquid saturation curve during freezing: influences of m and ΔTch (Zhou and Meschke 2013)

$$C\frac{\partial T}{\partial t} - L\frac{\partial \theta_i}{\partial t}\rho_i + \nabla(-\lambda \nabla T) = 0 \tag{1}$$

where T is the temperature (K), ρ_i is the density of ice, L is the latent heat of fusion of pore water per unit mass. Eq. (1) includes a term representing the energy released owing to the phase change of pore water during freezing. The effective heat capacity C and thermal conductivity λ of the soil are expressed as a function of the temperature (Eqs. (2) and (3)).

$$C = (1-n)\rho_s C_s + \theta_w \rho_w C_w + \theta_i \rho_i C_i \tag{2}$$

$$\log \lambda = \theta_s \log \lambda_s + \theta_w \log \lambda_w + \theta_i \log \lambda_i \tag{3}$$

where n is the porosity, θ is the volumetric fraction, and the subscripts s, w, and i represent the soil particles, pore water (or salt water), and ice, respectively. The volumetric fraction θ can be expressed as a function of χ_L and porosity n.

$$\theta_s = \frac{V_s}{V} = 1-n, \quad \theta_w = \frac{V_w}{V} = \chi_L n, \quad \theta_i = \frac{V_i}{V} = n(1-\chi_L) \tag{4}$$

where χ_L is the unfrozen liquid saturation. In this study, the unfrozen liquid content curve proposed by Zhou and Meschke (2013) was used. The slope and shape of the curve were determined based on the soil type.

$$\chi_L = \left(1 + \left(\frac{T_f - T}{\Delta T_{ch}}\right)^{\frac{1}{1-m}}\right)^{-m} \tag{5}$$

where ΔT_{ch} is the characteristic cooling temperature, m is an index indicating the pore radius distribution. The influence of ΔT_{ch} and m on the shape of the liquid saturation curve is illustrated in Fig. 2. T_f is freezing temperature of the soil (°C), and it tends to decrease nonlinearly as the salt concentration of the pore water increases. Kim and Go (2023) proposed the following empirical equation based on indoor experimental results to estimate the freezing point with different porewater salinity.

$$T_f = -0.5758 \cdot e^{0.408\zeta} + 0.535 \tag{6}$$

where ξ is salinity (%).

2.2 Establishment of artificial neural network

This study aims to build an ANN model to predict the required time to achieve the specific thickness of the freezing soil. In general, an ANN model has three layers: an input layer, a hidden layer, and an output layer.The input layer stores and provides data to the ANN network. In the hidden layer, which contains common neurons, connections are generated between the input and output layers. Each neuron in this hidden layer receives data from the input layer, which is essentially a weighted sum of the outputs from all the neurons in the previous layer. This sum is then transformed through a transfer function to generate a signal for the next layer. The output layer holds the predicted value generated by the network.

The total input value for each neuron can be estimated using the following equation.

$$z = Wx + b \tag{7}$$

The weight matrix (W) stores the weights connecting the current layer and the previous layer. The vector (x) and the vector (b) represents the output signal values from the prior layer, and the bias value at the current layer, respectively. In addition, the input values are processed within the neurons based on a transfer function. As a result, Eq. (7) can be expressed as follows.

$$y = f(Wx + b) \tag{8}$$

where f is non-linear function to improve the ANN model performance and better fit the data from input to output.

In this study, a tangent sigmoid transfer function $f(x) = 2/(1+e^{-2x})^{-1}$ is applied to all layers of the ANN model, except for the output layer, where a linear transfer function $f(x) = x$ is adapted. The transfer function enable the ANN network to generate the predicted value that closely match the expected values. If the transfer function were not used, the ANN model would only create the linear outputs. To ensure the network's performance, the Nguyen-Widrow method (Nguyen and Widrown 1990) was employed to determine the initial weights and biases.

There are two phases in the training procedure of the ANN model which are feed-forward and back-propagation calculation. In the feed-forward phase, the input data moves

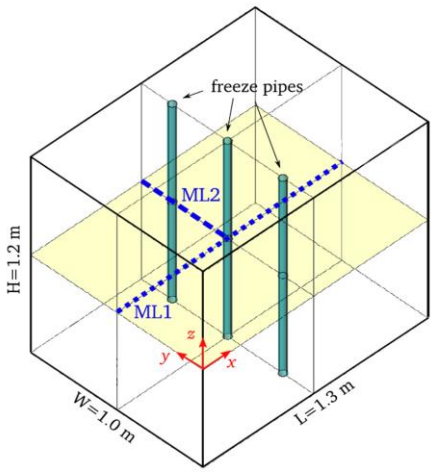

Fig. 3 Schematic of indoor laboratory tests (Marwan and Zhou 2016, Sres 2009)

from the input layer to the output layer by combining the output values of connected neurons in the previous layer. A transfer function is applied within each neuron to calculate the output value. Consequently, the output layer then estimates the predicted value. In addition, a cost function is used to measure the difference between the predicted value and the expected value from the dataset. In this article, the quadratic cost function is adapted and expressed as follows.

$$C = \sum (y_i - \exp_i)^2 \tag{9}$$

where y_i and $\exp_i$ are the predicted value estimated by the ANN and the expected value from the dataset, respectively.

During the back-propagation, the weight matrix is updated during each training step based on the loss function. This training process continues until the loss function is minimized. In each training iteration, a new weight matrix ($W+$) is estimated by considering the cost function and the current weight matrix (W).

$$W^+ = W - \eta \nabla C \tag{10}$$

where η is learning rate and is usually a small value. Meanwhile, ∇C is the slope of the cost function for the weights and can be calculated as follows.

$$\nabla C = [\partial C / \partial \omega_1 \ \cdots \ \partial C / \partial \omega_n]^T \tag{11}$$

In the training procedure, there are common which are overfitting and underfitting. Following these issues, the ANN model is overtrained with training data and fails to fit data with testing data. In this study, we investigated the effect of Bayesian regularization and Levenberg-Marquardt methods in solving these problems. These techniques are used to mitigate the overfitting and underfitting problems and enhance the predictive ability of the model on the testing data set.

Bayesian regularization is a method used to ensure the efficiency of ANN training. In general, the training process aims to minimize the loss function and is usually represented by the function $F = F_D$. However, Bayesian regularization requires additional terms to construct the objective function. This objective function in Bayesian Regularization can be expressed the following.

$$F = \chi E_D + \delta E_W \tag{12}$$

where E_D and E_w are the sum of squared errors and the sum of squared weights of the ANN model, respectively. In addition χ and δ are the parameters that can be obtained by the Gauss-Newton Approximation method.

The Levenberg-Marquardt technique is employed to address the non-linear least squares problem by combining the Gaussian-Newton method and the Steepest Descent method. The calculation of the new weights is performed using the following equation.

$$W_{t+1} = W_t - (J^T J + \eta I)^{-1} J^T E_i \tag{13}$$

In the equation provided, the identity unit matrix (I) is utilized along with a learning parameter (α) in the Levenberg-Marquardt technique. The Jacobian matrix (J) and the cumulative error vector (E) are key components in determining the cumulative error. When the learning rate (η) is set to 0, the Gauss-Newton method is employed, whereas the Steepest Descent method is utilized for larger learning rates. The learning rate (η) is automatically adjusted during each iteration. However, it is worth noting that the Levenberg-Marquardt technique has the drawback of requiring high computational costs due to the computation of large Jacobians and matrix inversions (Yoon *et al*. 2021).

3. Numerical modeling

3.1 Model validation

In this study, we utilized a data of indoor artificial freezing test carried out by Sres (2009) to validate the accuracy of a numerical simulation model developed for prediction of the artificial ground freezing behavior. By comparing the results of the numerical simulation to the experimental data obtained from the artificial freezing test, it was possible to validate the prediction reliability of the model in capturing the relevant physical mechanism. Sres (2009) carried out an indoor freezing experiment in a soil

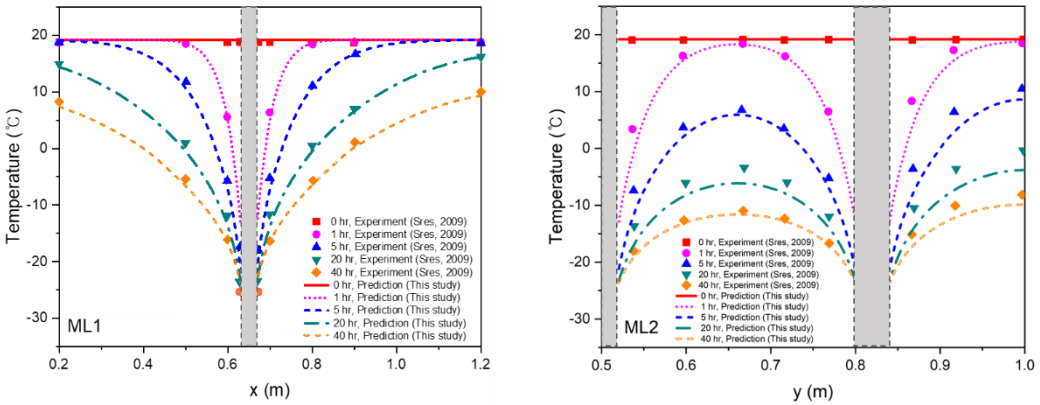

Fig. 4 Verification results: predicted temperature from the numerical simulation used in this study (plotted with a line), measured data (plotted with points)

bed filled with a saturated sandy soil for 40 h through three freeze pipes (the initial temperature was approximately 19°C). The temperature of the freeze pipe was maintained at -24°C. The soil temperature over time during the freezing process was measured by thermocouples installed on two observation lines (ML1, ML2 in Fig. 3). Fig. 4 shows that the simulation model reasonably estimated the indoor test observation results for the temperature change over time along the two observation lines.

3.2 Parametric study

This study aimed to investigate the impact of key parameters including the pore water salinity on the performance of artificial ground freezing using the constructed simulation model. In general, the salinity of pore water impacts the freezing behavior, including changes in the effective thermal conductivity. Oh *et al*. (2016) measured the effective thermal conductivity of a saturated sandy soil according to the salinity of pore water under frozen and unfrozen conditions. According to the measurement results of their studies, in the unfrozen soil, the effective thermal conductivity was measured to be between 2.11 and 2.22 W/(m·K) regardless of the salinity of pore water, which indicates that the effect of the salinity on the effective thermal conductivity was insignificant. However, in a frozen soil, the effective thermal conductivity was measured to be 3.79 W/(m·K) when a freshwater was considered and 4.48 W/(m·K) when a saltwater was considered, which was approximately 20% higher (Fig. 5).

They concluded that this phenomenon occurs as a result of desalinization, which occurs when salty pore water freezes, and that the precipitated salt in the solid state can increase the effective thermal conductivity of the frozen soil (Oh *et al*. 2016). In this study, the thermal conductivity of the soil particles was back-calculated to match the reported effective thermal conductivity and applied to the numerical analysis model. The effective thermal conductivities calculated by a numerical analysis are listed in Table 1. As the porosity range of the sample used in their thermal conductivity test was 0.4–0.5 (void ratio: 0.66–1.07) (Oh *et al*. 2016), a porosity of 0.4-0.5 was considered for this study.

Typically, in the field, artificial ground freezing is maintained until the soil temperature reaches approximately -3°C at the outer boundary of the design arch, where the thickness is typically considered to be 1.0 m (Konrad 1999; Yamamoto and Springman 2014). This study also considered target arch thickness as 1.0 m. Fig. 6 shows the example of simulation results of the ground temperature distribution under two different salinity conditions (freshwater, saltwater) at different time points. The predicted design wall reaching time was 197.5 h for the ground containing freshwater (salinity of 0‰) and 168 h for the ground containing saltwater (salinity of 35‰). This shows that the design ice wall reaching time may vary depending on the pore water salinity. The rate of ice wall formation is faster in soil containing salt water because the freeze-concentration effect caused by freezing increases the soil's effective thermal conductivity and accelerates the expansion rate of the ice column.

To examine the impact of key factors including the pore water salinity on the performance efficiency of the artificial ground freezing system, this study carried out a parametric study. As presented in Table 2, the study selected six key parameters and determined their corresponding ranges by reviewing parameters that had been the focus of previous studies (Hu *et al*. 2018, Chang and Lacy 2008, Holden 1997, Wang *et al*. 2019b). The pore water salinity used as key parameter in the parameter study was considered to range from 0 to 35‰, which is the theoretical range that can exist. Fig. 7 presents the model domain used for the parameter study, including the information of pipe spacing, initial temperature condition, and temperature boundary conditions at the freeze pipes wall. The domain size was set close to the field scale rather than the indoor testing scale, and the model includes 28,396 triangular finite elements. A freeze-pipe radius of 60–110 mm and the pipes spacing of 1.0 m were considered in the parametric study since freeze pipes are typically installed with a radius of 60-110 mm at intervals of 1.0-1.2 m in the field (Holden 1997, Wang *et al*. 2019b). The initial soil temperature was assigned in the

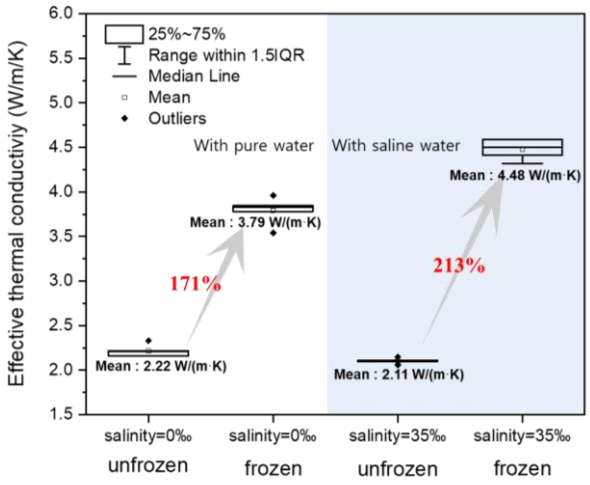

Fig. 5 Thermal conductivities of unfrozen and frozen soil samples in case of fresh pore water and saltwater; raw data were obtained from Oh *et al*. (2016)

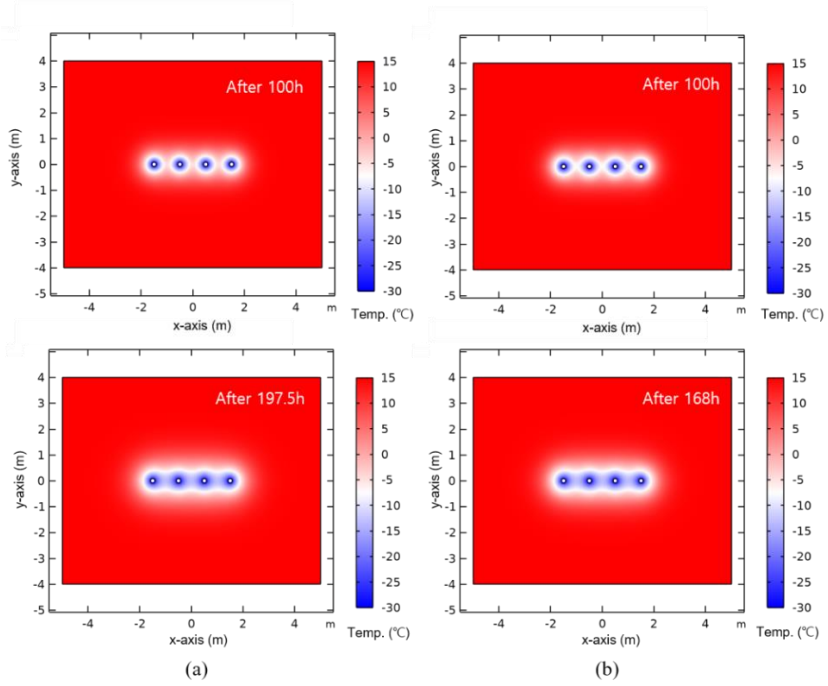

Fig. 6 Prediction results of the required time for target arch thickness (T_{pipe}=-30℃, T_i=15℃, λ_s=6.5W/(m·K), n=0.5, r_{pipe}=80 mm) (a) salinity= 0‰ and (b) salinity= 35‰)

Table 1 Calculated effective thermal conductivity in the simulation model

Property	Value	Unit
$\lambda_{eff,cal}$	2.22 $T \geq T_f$ (Salinity = 0‰) 2.22 $T \geq T_f$ (Salinity = 35‰) 3.80 $T < T_f$ (Salinity = 0‰) 4.50 $T < T_f$ (Salinity = 35‰)	W/(m · K)

range of 10–20℃, while the pipe wall of the freezing pipe was assigned a specific temperature condition in the range of -30 to -40℃. Thus, a total of 200 datasets were constructed using a combination of the selected parameters. When establishing the datasets, a Latin Hypercube Sampling technique was used as design for computer experiments, which produces a better uniformity in the set of points (McKay *et al*. 2000, Sacks *et al*. 1989). The results of a parametric study in Fig. 8 show linear trends between selected parameters and design wall reaching time.

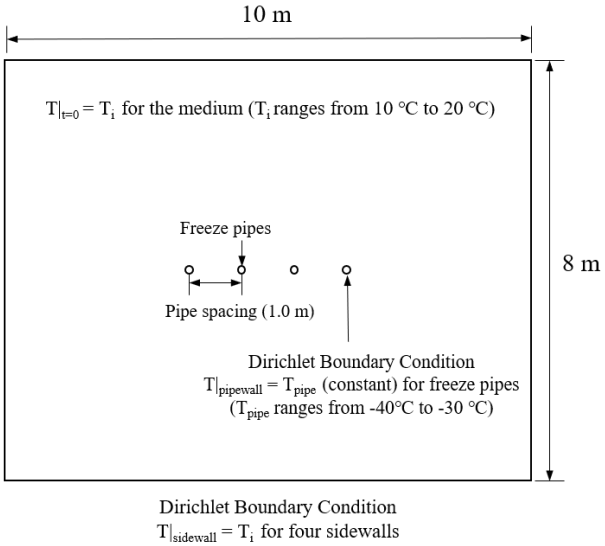

Fig. 7 Domain, boundary conditions, and initial condition of the numerical simulation model

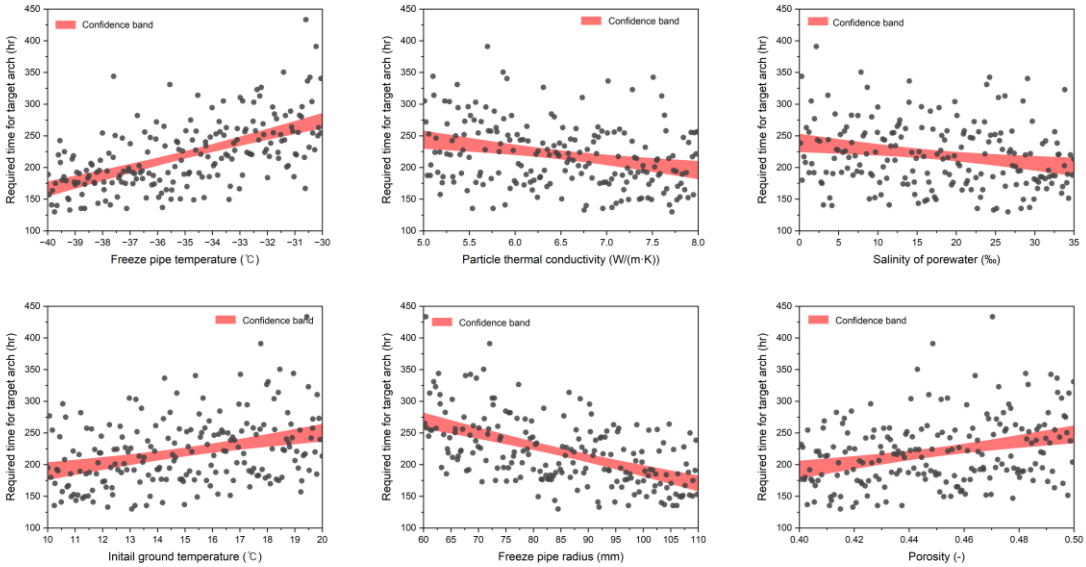

Fig. 8 Results of the parametric study under soil environmental and design conditions

Table 2 Ranges of selected parameters for the parametric study

Number	Parameter	Minimum	Maximum	Unit
1	Freeze pipe temperature	-40	-30	℃
2	Porosity	0.4	0.5	-
3	Particle thermal conductivity	5	8	W/(m・K)
4	Salinity	0	35	‰
5	Initial soil temperature	10	20	℃
6	Freeze pipe radius	60	110	mm

Here, the regression line is 95% confidence band. The higher the freezing pipe temperature, the lower the thermal conductivity of the soil particle, the lower the salinity of the pore water, the higher the initial ground temperature, the smaller the radius of the freezing pipe, and the larger the porosity, the more delayed the time for making target arch. Although there was some dispersion of data for each case, linear trends were observed from the derived regression bands, and hence the selected parameters should be considered as important factors. Before applying the

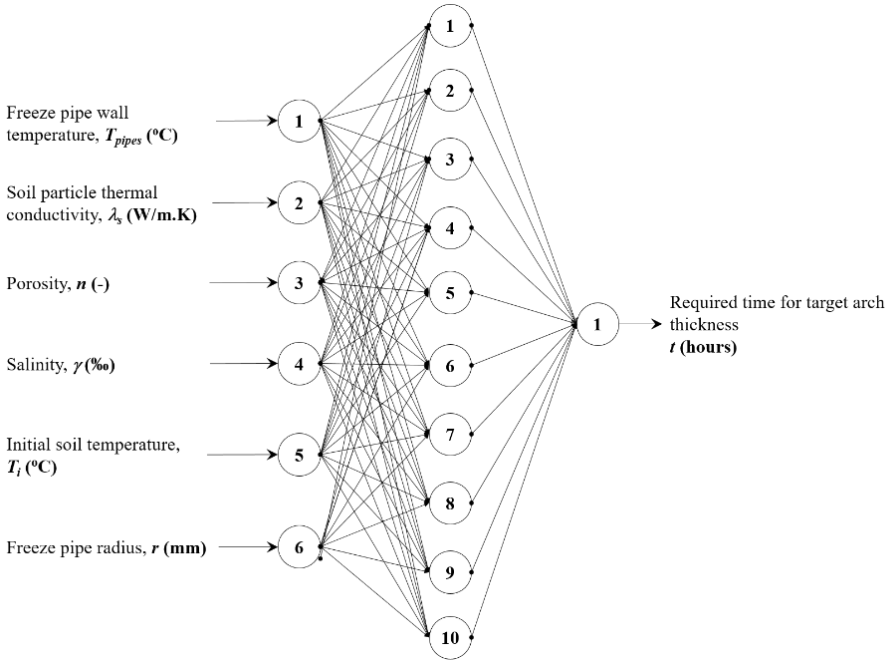

Fig. 9 Artificial neural network model for estimating the required time for target arch thickness

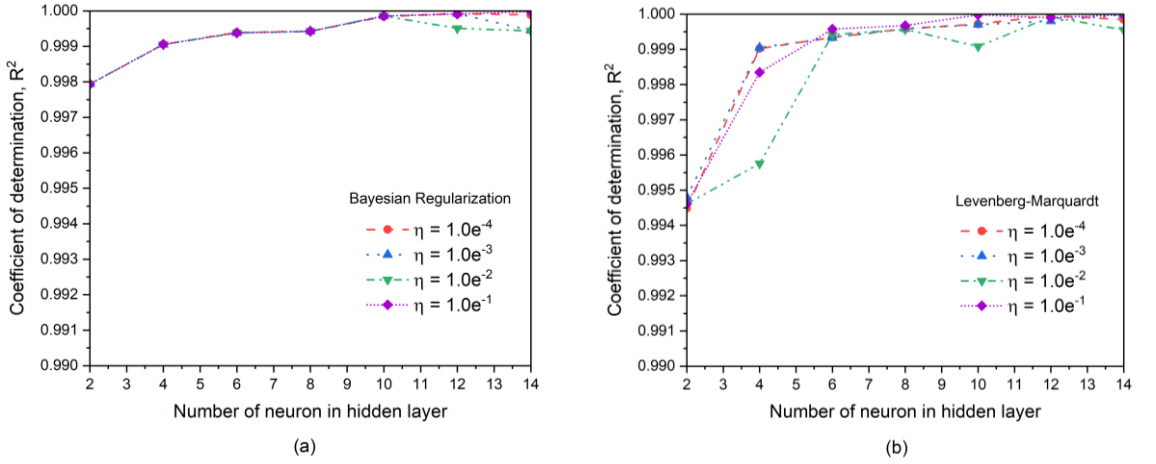

Fig. 10 Comparison of coefficient determination: (a) Bayesian Regularization and (b) Levenberg-Marquardt Training Process

artificial freezing method in the real field, it is required to check the target ground conditions through in-situ site investigation and then evaluate the most economical and efficient design method in advance.

3.3 Application of an ANN to predict desired time to reach the design wall

This study aims to construct an ANN model to predict the time required to achieve thickness of freezing soil in design step. The architecture of the ANN model as shown in Fig. 9, contains six neurons in the input layer, ten neurons in the hidden layer, and one neuron in the output layer. The collected dataset for ANN model includes 170 input-target pairs for training process and 30 pairs for testing. In order to improve the accuracy of the backpropagation phase and minimize the effect of overfitting and underfitting problems, Bayesian regularization and Levenberg-Marquardt techniques were investigated to select the proper technique for ANN model.

Fig. 10 illustrates the relationship between the coefficient of determination (R^2) and the number of neurons in the hidden layer for Bayesian Regularization and Levenberg-Marquardt, considering different learning rates (η = 10^{-4}, 10^{-3}, 10^{-2}, 10^{-1}). Overall, the coefficient of determination R^2 consistently converged to a very high value when the ANN model had more than six neurons in the hidden layer. Since the R^2 appeared stable for both algorithms at a learning rate of 10^{-1}, a training rate of 0.1 was employed in this study. Furthermore, it was observed from Fig. 11 that when the Levenberg-Marquardt algorithm was used, there was a significant difference in error and coefficients of determination between the training and testing sets. Additionally, the computation of the Jacobian

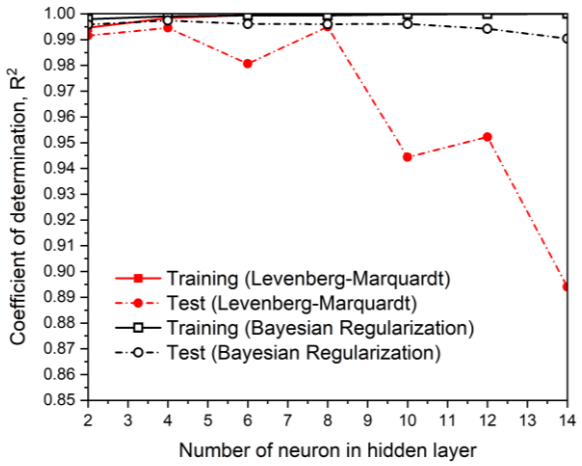

Fig. 11 Comparison of coefficient determination between training and testing results (when using Levenberg-Marquardt and Bayesian with learning rate of 0.1)

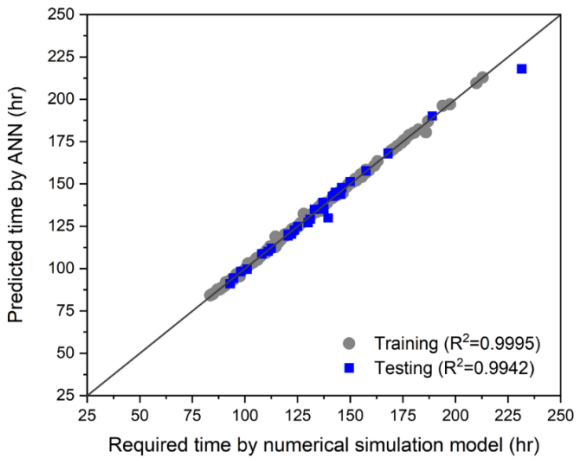

Fig. 12 Comparison results between the time required for the target arch predicted by the ANN model and the simulation model

matrix in the Levenberg-Marquardt algorithm led to higher computational costs. As a result, Bayesian regularization was finally adopted as an alternative approach in this study. By setting the learning rate to 0.1, the ANN model based on Bayesian regularization achieved the highest R^2 value, and the error of R^2 between training and testing was minimized with 10 neurons in the hidden layer. Hence, the learning rate and the number of neurons in the hidden layer were set to 0.1 and 10, respectively.

Before using the ANN model in the application, the trained ANN model needs to be evaluated with a test dataset that has never been used in the training procedure. Figure 12 shows the comparison between the time required for the desired arch predicted by the ANN model and the simulation model. The ANN model demonstrated high accuracy with R^2 values of 0.9995 for the training data and 0.9942 for the test data. This investigation indicates that the proposed ANN-based prediction model is reliable and suitable for estimating the time required for the target arch thickness. To assess the sensitivity and significance of the input parameters employed in constructing the ANN model, this study employed the Garson analysis (Garson 1991). This analysis technique shows the distribution of connection weights between layers of an ANN, providing valuable insights into the important features corresponding to the input variables of the ANN model. The distribution of connection weights from input to output of an ANN model can be determined as follows.

$$\frac{\sum_j^{N_H}\left(\frac{I_{V_j}}{\sum_k^{N_V} I_{V_j}} O_j\right)}{\sum_i^{N_V}\sum_j^{N_H}\left(\frac{I_{V_j}}{\sum_k^{N_V} I_{V_j}} O_j\right)} \tag{13}$$

where N_H and N_V are the number of the neurons in the

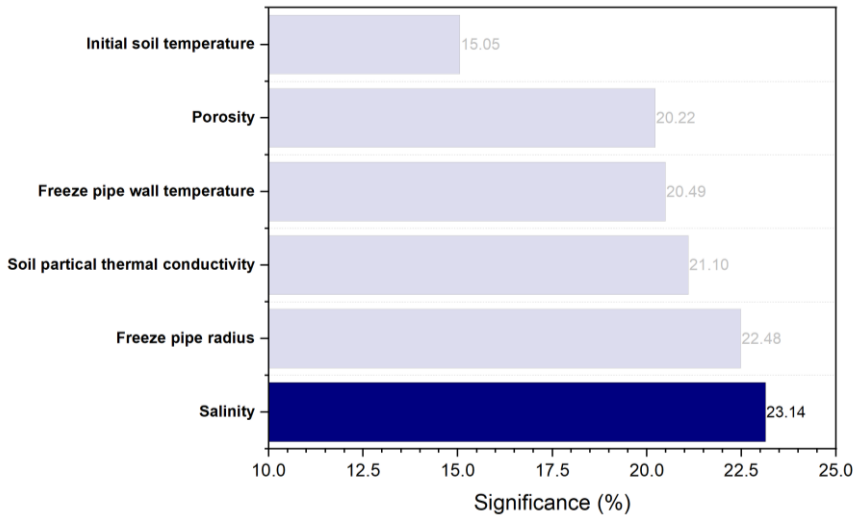

Fig. 13 Feature significance plot based on Garson analysis

hidden layers and the number of the variable (input parameters). I_V represents the summation of the product of input connection weights in the hidden layer, while O denotes the connection weight of the output node. Table 3 presents the interpretation of the connection weights and biases for each layer. Following the Table 3, there are three subsections: Connection Weights, Absolute Connection Weights, and Connection Shares Multiple with Hidden Node Input. The Connection Weights section describes the weight matrices of the ANN model, while the remaining two parts show the calculation based on the Garson analysis procedure using Eq. (13). The columns "Para 1" through "Para 6" correspond to the connections originating from the input parameters of the ANN network: Freezing pipe wall temperature T_{pipes}, Soil particle thermal conductivity λ_s, Porosity n, Salinity γ, Initial soil temperature T_i, and Freeze pipe radius r. These parameters correspond to the first through sixth nodes in the input layer of the ANN network, as shown in Fig. 9. In addition, the hidden layer consists of 10 nodes, and the output layer has one node, therefore, the ANN network includes two weight matrices. The first weight matrix, connecting the input layer and the hidden layer, has a size of 10×6 corresponding to columns "Para 1" to "Para 6" in the Connection Weights section. The second weight matrix, connecting the hidden layer and the output layer, has a size of 1×10 and is shown in the "OUT" column corresponding to 10 values of the weight matrix.

7. Conclusions

To achieve an efficient design of artificial ground freezing systems, fundamental numerical analyses studies are required to investigate the freezing behavior of soil under various environmental conditions as well as design conditions. In this study, numerical simulation model was used to examine the impact of key parameters on the efficiency of artificial ground freezing process in a saturated soil bed containing saltwater. Then, a parametric study was carried out to analyze the variables that affect the formation of design of ice walls. Lastly, based on the dataset from the parametric study, a new prediction model based on artificial neural network technique was proposed that can predict the required time for achieving the desired arch thickness more practically. The main conclusions drawn from the study results can be summarized as follows.

- The reliability of the numerical simulation model used in this study was evaluated by comparing its predictions to the results of laboratory artificial ground freezing tests in prior studies. The verification results confirmed that the simulation model reasonably predicted the freezing behavior of the soil.
- The study carried out a parametric study to examine the impact of key factors including the pore water salinity on the performance efficiency of the artificial ground freezing system. The results of a parametric study showed that when using artificial ground freezing to create a target arch, the required time tended to be reduced with varying certain conditions: lower freeze pipe temperature, lower initial ground temperature, lower soil porosity, higher particle thermal conductivity, higher pore water salinity, and higher freeze pipe radius.
- After evaluating the sensitivity of each parameter to artificial ground freezing behavior through multiple statistical analyses, an artificial neural network model was proposed that can practically estimate the required time for achieving the desired arch thickness. According to the interpreting connection weights, the salinity in the pore water emerged as the most influential input factor, whereas the initial soil temperature exhibited the least importance. The ANN model has high accuracy (R^2 = 0.9942) in predicting the time required to achieve the desired arch thickness for the testing data set. The trained ANN model has high accuracy in the prediction task with the test data set that was separated independently from the training data. This demonstrates the strong ability of the ANN model to predict new independent data.

Table 3 Garson analysis results

Hidden node	Para 1	Para 2	Para 3	Para 4	Para 5	Para 6	OUT
Connection weights (Input to hidden)							
1	0.2681	0.4294	0.1217	-0.5774	-0.0166	-0.9519	0.5316
2	0.1027	-0.4003	-0.3371	-0.8539	-0.3481	0.8808	-0.4000
3	0.2723	0.3066	0.1206	0.5837	-0.0338	0.2007	-0.4439
4	0.2428	0.3456	0.1372	-0.3690	-0.1519	-1.1328	-0.5037
5	-0.6084	0.3281	-0.2011	0.1741	-0.2342	-0.0418	0.7438
6	0.3412	0.1412	-0.4541	0.3097	0.4352	0.2720	-0.2563
7	-0.0036	-0.4630	-1.5588	0.3604	0.9787	0.4646	-1.0152
8	0.3506	0.2449	0.6746	0.7079	0.2539	-0.4962	-0.6045
9	0.2018	0.3335	0.3449	0.3098	-0.0246	-0.0052	0.9913
10	-0.9472	0.5223	-0.0049	-0.1955	0.6102	-0.1399	0.9919
Absolute connection weights (input to hidden)							
1	0.2681	0.4294	0.1217	0.5774	0.0166	0.9519	0.5316
2	0.1027	0.4003	0.3371	0.8539	0.3481	0.8808	0.4000
3	0.2723	0.3066	0.1206	0.5837	0.0338	0.2007	0.4439
4	0.2428	0.3456	0.1372	0.3690	0.1519	1.1328	0.5037
5	0.6084	0.3281	0.2011	0.1741	0.2342	0.0418	0.7438
6	0.3412	0.1412	0.4541	0.3097	0.4352	0.2720	0.2563
7	0.0036	0.4630	1.5588	0.3604	0.9787	0.4646	1.0152
8	0.3506	0.2449	0.6746	0.7079	0.2539	0.4962	0.6045
9	0.2018	0.3335	0.3449	0.3098	0.0246	0.0052	0.9913
10	0.9472	0.5223	0.0049	0.1955	0.6102	0.1399	0.9919
Connection shares × hidden node input							
1	0.1009	0.1615	0.0458	0.2172	0.0062	0.3581	
2	0.0201	0.0784	0.0660	0.1672	0.0682	0.1725	
3	0.0918	0.1033	0.0407	0.1967	0.0114	0.0677	
4	0.0981	0.1397	0.0554	0.1491	0.0614	0.4578	
5	0.2927	0.1578	0.0968	0.0838	0.1127	0.0201	
6	0.0520	0.0215	0.0692	0.0472	0.0664	0.0415	
7	0.0011	0.1397	0.4703	0.1088	0.2953	0.1402	
8	0.0950	0.0663	0.1827	0.1918	0.0688	0.1344	
9	0.1647	0.2722	0.2815	0.2529	0.0201	0.0042	
10	0.4121	0.2272	0.0021	0.0850	0.2655	0.0609	
Sum:	1.3285	1.3678	1.3105	1.4997	0.9759	1.4574	
Input node share of output layer connections, excluding bias ones							
	Para 1	Para 2	Para 3	Para 4	Para 5	Para 6	
	20.49%	21.10%	20.22%	23.14%	15.05%	22.48%	

Acknowledgments

This work was supported by the National Research Foundation of Korea(NRF) grant funded by the Korea government(MSIT) (No. 2022R1C1C1006507).

References

Alzoubi, M.A., Xu, M., Hassani, F.P., Poncet, S. and Sasmito, A.P. (2020), "Artificial ground freezing: A review of thermal and hydraulic aspects", *Tunn. Undergr. Sp. Tech.*, **104**, 103534-1-18. https://doi.org/10.1016/j.tust.2020.103534.

Andersland, O.B. and Ladanyi, B. (2004), Frozen ground engineering (Second edition), John & Wiley Sons.

Chang, D.K. and Lacy, H.S. (2008), "Artificial ground freezing in geotechnical engineering", *Proceedings of the 6th International Conference on Case Histories in Geotechnical Engineering*.

Cicchetti L. (2018), Thermo-hydro-mechanical simulations of artificial ground freezing, MSc thesis, Departments of Civil and Environmental Engineering at NTNU and DTU.

Comsol (2024), Introduction to Comsol Multiphysics, Comsol, Inc., USA.

Coussy O. (2010), Mechanics and physics of porous solids. John Wiley and Sons..

Coussy O. (2004), Poromechanics. John Wiley & Sons: Chichester, UK.

Coussy, O. and Monteiro, P. (2007), "Unsaturated poroelasticity for crystallization in pores", *Com. Geotech.*, **34**(4), 279-290.

https://doi.org/10.1016/j.compgeo.2007.02.007.
Crippa, C. and Manassero, V. (2006), "Artificial ground freezing at Sophiaspoortunnel (The Netherlands). Freezing parameters: data acquisition and processing", *Proceeding of the GeoCongress 2006: Geotechnical Engineering in the Information Technology Age*, Civil Engineering in the Arctic Offshore, Atlanata, 1-6. https://doi.org/10.1061/40803(187)254.
Garson, G.D. (1991), Interpreting Neural Network Connection Weights. AI Expert.
Han, L., Ye, G., Li, Y., Xia, X. and Wang, J. (2016), "In situ monitoring of frost heave pressure during cross passage construction using ground-freezing method", *Can. Geotech. J.*, **53**, 530-539. https://doi.org/10.1139/cgj-2014-0486.
Hansson, K., Šimuˇnek, J., Mizoguchi, M., Lundin, L.C. and Van Genuchten, M.T. (2004), "Water flow and heat transport in frozen soil", *Vadose Zone J.*, **3**, 693-704. https://doi.org/10.2113/3.2.693.
Holden, J.T. (1997), "Improved thermal computations for artificially frozen shaft excavations", *J. Geotech. Geoenviron. Eng*., **123**(8), 696-701. https://doi.org/10.1061/(ASCE)1090-0241(1997)123:8(696).
Hu, R.; Liu, Q. and Xing, Y. (2018), "Case study of heat transfer during artificial ground freezing with groundwater flow", *Water*, **10**, 1322. https://doi.org/10.3390/w10101322.
Huang, S., Guo, Y., Liu, Y. Ke, L., Liu, G. and Chen, C. (2018), "Study on the influence of water flow on temperature around freeze pipes and its distribution optimization during artificial ground freezing", *Appl. Therm. Eng.*, **135**, 435-445. https://doi.org/10.1016/j.applthermaleng.2018.02.090.
Jin, H., Go, G.H., Ryu, B.H. and Lee, J. (2021), "Experimental and numerical investigation of closure time during artificial ground freezing with vertical flow", *Geomech. Eng*., **27**(5), 433-445. https://doi.org/10.12989/gae.2021.27.5.433.
Kim, H.W. and Go, G.H. (2023), "Measurement and verification of unfrozen water retention curve of frozen sandy soil based on pore Water Salinity" *J. the Kor. Geotech. Soci*., **39**(11), 53-62. https://doi.org/10.7843/kgs.2023.39.11.53
Konrad, J.M., (1999), "Frost susceptibility related to soil index properties", *Can. Geotech. J.*, **36**, 403-417. https://doi.org/10.1139/t99-008.
Kurylyk, B.L., McKenzie, J.M., MacQuarrie, K.T. and Voss, C.I. (2014), "Analytical solutions for benchmarking cold regions subsurface water flow and energy transport models: one-dimensional soil thaw with conduction and advection", *Adv. Water Res.*, **70**, 172-184. https://doi.org/10.1016/j.advwatres.2014.05.005.
Li, C.C., Kristjansson, G. and Høien, A.H. (2016), "Critical embedment length and bond strength of fully encapsulated rebar rockbolts", *Tunn. Undergr. Sp. Tech.*, **59**, 16-23. https://doi.org/10.1016/j.tust.2016.06.007.
Li, Z., Chen, J., Sugimoto, M. and Ge, H. (2019), "Numerical simulation model of artificial ground freezing for tunneling under seepage flow conditions", *Tunn. Undergr. Sp. Tech.*, **92**, 103035. https://doi.org/10.1016/j.tust.2019.103035
Lunardini, V.J. (1998), "Effect of convective heat transfer on thawing of frozen soil", (Eds., Lewkowicz, A.G. and Allard, M.) *Proceedings of the seventh international conference on permafrost*, Canada: Yellowknife.
Marwan, A., Zhou, M., Abdelrehim, M.Z. and Meschke, G. (2016), "Optimization of artificial ground freezing in tunneling in the presence of seepage flow", *Com. Geotech.*, **75**, 112-125. https://doi.org/10.1016/j.compgeo.2016.01.004.
McKay, M.D., Beckman, R.J. and Conover, W.J. (2000), "A comparison of three methods for selecting values of input variables in the analysis of output from a computer code", *Technometrics*, **42**(1), 55-61. https://doi.org/10.2307/1268522.
McKenzie, J.M., Voss, C.I. and Siegel, D.I. (2007), "Groundwater flow with energy transport and water–ice phase change: numerical simulations, benchmarks, and application to freezing in peat bogs", *Adv. Water Resour.*, **30**(4), 966-983. https://doi.org/10.1016/j.advwatres.2006.08.008.
Michalowski, R.L. and Zhu, M. (2006), "Frost heave modelling using porosity rate function", *Int. J. Numer. Anal. Method. Geomech.*, **30**(8), 703-722. https://doi.org/10.1002/nag.497.
Naithani, A.K., Jain, P., Singh, L.G. and Rawat, D.S. (2022), "Engineering geological characteristics of the underground surge pool cavern: A case study, India", *Int. J. Geo-Eng.*, **13**(1), 7. https://doi.org/10.1186/s40703-022-00172-9.
Nguyen, D. and Widrow, B. (1990), "Improving the learning speed of 2-layer neural networks by choosing initial values of the adaptive weights", *Proceedings of the International Joint Conference on Neural Networks*, San Diego, CA, USA.
Oh, M., Lee, D., Son, Y.J., Lee, I.M. and Choi, H. (2016), "Effect of pore-water salinity on freezing rate in application of rapid artificial ground freezing to deep subsea tunnel: concentration of laboratory freezing chamber test", *J. Kor. Tunn. Undergr, Sp. Assoc.*, **18**(5), 401-412. http://dx.doi.org/10.9711/KTAJ.2016.18.5.401.
Osgoui, R.R. and Ünal, E. (2009), "An empirical method for design of grouted bolts in rock tunnels based on the Geological Strength Index (GSI)", *Eng. Geol.*, **107**(3-4), 154-166. https://doi.org/10.1016/j.enggeo.2009.05.003.
Papakonstantinou, S., Anagnostou, G. and Pimentel, E. (2013), "Evaluation of ground freezing data from the Naples subway", *Proceedings of the Institution of Civil Engineers-Geotechnical Engineering*, **166**(3), 280-298.
Pimentel, E., Papakonstantinou, S. and Anagnostou, G. (2012), "Numerical interpretation of temperature distributions from three ground applications in urban tunnelling", *Tunn. Undergr. Sp. Tech.*, **28**, 57-69. https://doi.org/10.1016/j.tust.2011.09.005.
Sacks, J., Welch, W.J., Mitchell, T.J. and Wynn. H.P. (1989), "Design and analysis of computer experiments", *Statist. Sci*. **4**(4), 409-423.
Schmall, P. and Dawson, A. (2017), "Ground-freezing experience on the east side access Northern Boulevard crossing, New York", *Proceedings of the Institution of Civil Engineers - Ground Improvement* , **170**(3), 159-172
Shen, Y., Wang, Y., Zhao, X., Yang, G., Jia, H. and Rong, T. (2018), "The influence of temperature and moisture content on sandstone thermal conductivity from a case using the artificial ground freezing (AGF) method", *Cold Reg. Sci. Technol*., **155**, 149-160. https://doi.org/10.1016/j.coldregions.2018.08.004.
Shin, H., Kim, J. and Lee, J (2018), "Effect of groundwater flow on ice-wall integrity", *J. Korean Geotech. Soc.*, **34**(11), 43-55. https://doi.org/10.7843/kgs.2018.34.11.43.
Sres, A. (2009), Theoretische und experimentelle Untersuchungen zur Künstlichen Bodenvereisung im Strömenden Grundwasser, Ph.D. thesis, ETH Zürich.
Tacim, G., Posluk, E. and Gokceoglu, C. (2023), "Importance of grouting for tunneling in karstic and complex environment (a case study from Türkiye)", *Int. J. Geo-Eng.*, **14**(1), 6. https://doi.org/10.1186/s40703-023-00183-0
Tan X.J., Chen, W.Z., Tian, H.M. and Cao, J.J. (2011), "Water flow and heat transport including ice/water phase change in porous media: numerical simulation and application", *Cold Reg. Sci. Technol.*, **68**(12), 74-84. https://doi.org/10.1016/j.coldregions.2011.04.004.
Tounsi, H., Rouabhi, A. and Jahangir, E. (2020), "Thermo-hydro-mechanical modeling of artificial ground freezing taking into account the salinity of the saturating fluid", *Com. Geotech.*, **119**, 103382. https://doi.org/10.1016/j.compgeo.2019.103382.
Vitel, M., Rouabhi, A., Tijani, M. and Guerin, F. (2016), "Modeling heat and mass transfer during ground freezing subjected to high seepage velocities", *Com. Geotech*, **73**, 1-15.

https://doi.org/10.1016/j.compgeo.2015.11.014

Wang, H., Li, S., Wang, Q., Wang, D., Li, W., Liu, P., Li, X. and Chen, Y. (2019a), "Investigating the supporting effect of rock bolts in varying anchoring methods in a tunnel", *Geomech. Eng*., **19**(6), 485-498. https://doi.org/10.12989/gae.2019.19.6.485.

Wang, B., Rong, C.X., Lin, J., Cheng, H. and Cai, H.B. (2019b), "Study on the formation law of the freezing temperature field of freezing shaft sinking under the action of large-flow-rate groundwater", *Adv. Mater. Sci. Eng*., https://doi.org/10.1155/2019/1670820.

Wu, M., Tan, X., Huang, J., Wu, J. and Jansson, P.E. (2015), "Solute and water effects on soil freezing characteristics based on laboratory experiments", *Cold Reg. Sci. Technol.*, **115**, 22-29. https://doi.org/10.1016/j.coldregions.2015.03.007.

Yamamoto, Y. and Springman, S.M., (2014), "Axial compression stress path tests on artificial frozen soil samples in a triaxial device at temperatures just below 0°C", *Can. Geotech. J*., **51**, 1178-1195. https://doi.org/10.1139/cgj-2013-0257.

Yoon, S., Le, D.V. and Go, G.H. (2021) "Artificial neural network-based model for prediction of frost heave behavior of silty soil specimen", *Appl. Sci*., **11**, 10834. https://doi.org/10.3390/app112210834.

Zhou, J. and Tang, Y. (2018), "Experimental inference on dualporosity aggravation of soft clay after freeze-thaw by fractal and probability analysis", *Cold Reg. Sci. Technol.*, **153**, 181-196. https://doi.org/10.1016/j.coldregions.2018.06.001.

Zhou, M.M. and Meschke, G. (2013), "A three-phase thermo-hydro-mechanical finite element model for freezing soils" *Int. J. Numer. Anal. Method. Geomech.*, **37**(18), 3173-3193. https://doi.org/10.1002/nag.2184.

Zhou X., Liu, X., Xiao, Y., Liang, N., Yang, Y., Han, Y. and Yang, Z., (2023), "Analysis of stability control and the adapted ways for building tunnel anchors and a down-passing tunnel", *Geomech. Eng*., **35**(4), 395-409. https://doi.org/10.12989/gae.2023.35.4.395.

IC